PAPER • OPEN ACCESS

Isomer-dependent vibrational coherence in ultrafast photoisomerization

To cite this article: J Léonard *et al* 2013 *New J. Phys.* **15** 105022

New Journal of Physics
The open access journal for physics

Isomer-dependent vibrational coherence in ultrafast photoisomerization

J Léonard[1], J Briand[1], S Fusi[2], V Zanirato[3], M Olivucci[2,4] and S Haacke[1,5,6]

[1] Institut de Physique et Chimie des Matériaux de Strasbourg and LabEX NIE, UMR 7504 Université de Strasbourg—CNRS, F-67034 Strasbourg, France
[2] Dipartimento di Chimica, Università degli Studi di Siena, I-53100 Siena, Italy
[3] Dipartimento di Scienze Farmaceutiche, Università di Ferrara, I-44100 Ferrara, Italy
[4] Chemistry Department, Bowling Green State University, Bowling Green, OH 43403, USA
E-mail: stefan.haacke@ipcms.u-strasbg.fr

New Journal of Physics **15** (2013) 105022 (17pp)
Received 30 July 2013
Published 23 October 2013
Online at http://www.njp.org/
doi:10.1088/1367-2630/15/10/105022

Abstract. Molecular switches based on the *N*-alkylated indanylidene-pyrroline (NAIP) framework mimic some of the outstanding double bond photoisomerization properties of retinal Schiff bases in rhodopsin, most notably, the occurrence of vibrational coherences in the excited and photoproduct ground states. Focusing on the zwitterionic NAIP switch and using broadband transient absorption spectroscopy, our previous investigation of the *Z* to *E* photoisomerization dynamics is now extended to the study of the backward *E* to *Z* photoisomerization and to the role of the solvent on the vibrational coherence accompanying the photoreaction. Despite very similar signatures of excited-state vibrational coherence and similar isomerization times, the backward reaction has a significantly smaller isomerization yield than the forward reaction, and most interestingly, does not display ground state coherences. This indicates that both the quantum yield and vibrational dephasing depend critically on

[5] IPCMS-DON, 23, rue du Loess, 67034 Strasbourg Cedex, France.
[6] Author to whom any correspondence should be addressed.

the photochemical reaction path followed to reach the ground potential energy surface. In addition, investigation of the effect of the solvent viscosity shows that vibrational dephasing is mainly an intramolecular process.

S Online supplementary data available from stacks.iop.org/NJP/15/105022/mmedia

Contents

1. Introduction

Double bond photoisomerization is a light-triggered chemical reaction leading to structural changes at the nanoscale. In recent years, synthetic chromophores capable of undergoing such a chemical event have found an increasing number of opto-electronic and biophysical applications yielding novel photoresponsive materials. Nevertheless, in living systems a highly specialized chromophore, the protonated Schiff base of retinal, has been selected by the biological evolution to control a series of basic functions such as vision, circadian rhythm, ion-channels, light energy conversion. When incorporated in the protein (opsin) environment of the dim-light visual pigment rhodopsin (Rh), the retinal chromophore displays outstanding properties in terms of isomerization quantum yield (65%) and speed (200 fs). Most remarkably, Rh provides the only natural example of a vibrationally coherent photoisomerization [1]. This process is of particular interest since the coherent photoisomerization funnels a significant amount of the absorbed photon energy into a limited number of vibrational modes in the electronic ground state thus transducing light-energy into mechanical-energy at the molecular level. Therefore, Rh appears to provide a model system for a molecular opto-mechanical transducer operating efficiently in the condensed phase.

Vibrational coherence originates from the coupling of two molecular electronic states by an ultrashort laser pulse. Raman-active vibrational modes are populated and phase coherence between vibrational states is imposed by the coherent laser field in both electronic states [2–5]. This yields vibrational wavepackets which may oscillate in their electronic potential well provided their period is simultaneously longer than the laser pulse duration, and shorter than the vibrational dephasing time and the electronic state lifetime. Vibrational wavepackets have

been observed in a variety of photoisomerizing molecules and their time-resolved spectroscopic signatures are oscillatory signals, non-exponential kinetics or dynamics spectral shifts [1, 6–21].

Remarkably, even in condensed phase, where dephasing is extremely fast, there are a few examples of photoreactions displaying vibrational coherence in non-Raman-active modes [22], or in electronic states other than those initially coupled by the light pulse and in particular in the product of an ultrafast photoreaction [1, 23, 24]. In the latter case, the reactive motion imposed by the topology of the excited electronic potential energy on the light-induced wavepacket generates vibrational coherence in other, usually low-frequency modes involved in the reaction coordinate, leading to a so-called coherent photochemical reaction.

Recent advances in quantum chemistry have enabled the computation of quantum mechanics/molecular mechanics (QM/MM) trajectories revealing the excited state structural dynamics of molecules as complex as Rh at the individual atomic level, with high temporal resolution [18, 25], and in good agreement with observations [6]. It is even possible to pursue the trajectory computation after the non-adiabatic decay to the ground state through a conical intersection (CI) [18, 20, 26] where the branching ratio is controlled. This opens the way toward accurate comparison with the observed photoproduct dynamics and possibly quantum yield prediction.

In this context, we have been investigating both by *ab initio* quantum chemistry methods and femtosecond spectroscopy [19, 20, 27–29] a family of *N*-alkylated indanylidene-pyrroline (NAIP) photoswitches which are mimicking the photochemistry of retinal Schiff bases in Rh. These photo-isomerizing model systems are small enough to be entirely treatable by QM/MM techniques, including the solvent. At the CASPT2/CASSCF QM level, the excited state potential energy surface is barrierless along torsion around the central double bond, and a CI is situated at almost 90° torsion [27]. As shown experimentally, this leads to isomerization times as short as 0.2–0.5 ps depending on substitutions on the indanone moiety, and with quantum yields in the range of 0.20–0.35 [19, 20, 28, 30]. Most importantly, the molecules showing the shortest excited-state lifetimes also display signatures of coherent excited and photoproduct wavepacket dynamics [19, 20], similar to those reported for Rh. Semi-classical trajectory computations of the indanylidene-pyrroline (IP) compounds indicate that the observed ground state oscillations are the signature of coupled double-bond twisting and ring-inversions [20] and, that the isomerization proceeds with vibrational coherence along the reaction coordinate. The IP compounds thus appear as a model system to investigate the conditions for the appearance of vibrational coherence along the reaction motion, and its implication in terms of reaction speed and yield.

Here, we report new results on the wavepacket dynamics triggered by barrierless photoisomerization in the dipolar ZW-NAIP. We compare the dynamics of the backward *E* to *Z* photoreaction to that of the forward *Z* to *E* reaction, and investigate possible solvent effects for the forward reaction. Interestingly, while the observed reaction and excited state dynamics are very similar in both directions, the quantum yield is significantly different, and the ground state wavepacket observed in the *Z* to *E* direction is no longer observed in the backward direction. In addition, studying the forward reaction in a few selected alcohols, among which the higher viscosity decanol, reveals hardly any change in the reaction dynamics and vibrational coherence. This suggests that the vibrational coherence is observed in a so-called volume-conserving deformation in line with the ring inversion modes predicted by QM/MM semi-classical trajectory computations [20], and that vibrational dephasing is in essence an intramolecular process in this compound.

2. Experimental methods

The home-built, broadband (300–1000 nm) transient absorption (TA) set-up is described in details in [19]. Briefly, it is based on a 5 kHz Ti:sapphire amplified laser delivering 40 fs, 0.5 mJ output pulses. The pump wavelength is obtained by second harmonic generation. It is fixed at 400 nm, with an intensity kept in the linear regime of excitation, so as to promote not more than 5% of the ZW-NAIP molecule (*Z* or *E* isomer form) to its first excited electronic state S_1 (see figure 1(A)). The time resolution is 80 fs (FWHM of the solvent Raman response). Experiments are performed on a 5–10 ml solution continuously circulated through a 0.5 mm thin fused silica capillary. The concentration ($\approx$0.5 mM) is adjusted to have an optical density of $\approx$0.6 at 400 nm. Steady-state absorption spectra are measured shortly before and after TA acquisition using a UV–Vis spectrophotometer (U-3000, Hitachi). No sign of photo-degradation is observed and the change in isomer content is small, not larger than 10% relative to the initial isomer ratio (see below). All TA data presented in this paper are processed following the procedure described in [19] in order to compensate for group velocity dispersion and define time zero within $\pm$20 fs over the entire detection spectral range. Quantitative analysis methods are described in the SI of [20].

The comparative study of the dynamics observed when exciting the *Z* or the *E* isomers is performed on deuterated methanol (CD_3OD, Sigma-Aldrich) solutions. A single stock solution of concentration $\sim$5 mM is prepared. Half of the volume is kept in the dark, the second half is irradiated with an argon laser over night. The isomer content of both samples is determined by recording ^{1}H-NMR spectra on a 300 MHz spectrometer (Avance 300 MHz, Bruker). Immediately after, the samples are diluted by 10 and TA measurements are performed on both samples one after the other. Figure 1 shows the structure, H-NMR and UV–Vis absorption spectra of ZW-NAIP in both *Z*- and *E*-enriched solutions. The *Z* isomer is the more stable and accumulates up to $>$98% at room temperature in the dark, as determined by H-NMR spectroscopy (B). Upon illumination at 454.6 nm a steady-state isomer mixture of 12% *Z* and 88% *E* is obtained. At room temperature in the dark, this ratio relaxes to pure *Z* with a time constant $>$10 h, allowing for TA experiments to be performed on the *E* isomer. Note that the 400 nm pump pulses slightly favors excitation of the *E*-form since its extinction coefficient is larger by a factor 1.09 (figure 1(C)). The isosbestic point is situated at 410 nm.

To investigate the effect of solvent viscosity protonated methanol, butanol and decanol are used as received (Sigma-Aldrich). TA experiments are performed on the *Z* isomer only (solutions kept in the dark).

3. Results and analysis

3.1. Vibrationally coherent photoizomerization in the forward Z to E direction

Figure 2 displays the TA obtained for the *Z*-enriched, CD_3OD solution of ZW-NAIP. Within experimental noise, the data for the forward reaction is identical to that observed in CH_3OH and already discussed in detail in [19]. Before presenting new results pertaining to the backward (*E* to *Z*) reaction and to the solvent influence, we recall here the main features of the forward reaction highlighting the non-exponential kinetics and coherent dynamics:

- Stimulated emission (SE) occurs within the temporal instrument response function at $\lambda > 460$ nm (figure 2(A)).

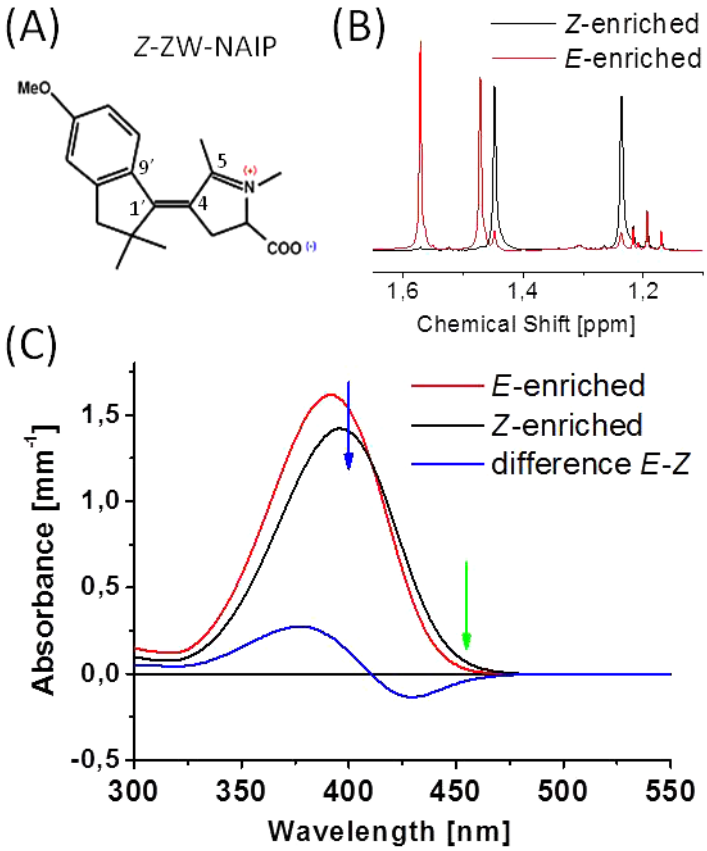

Figure 1. (A) Schematic structure of ZW-NAIP in the *Z* isomer. (B) ^{1}H-NMR spectra showing that the *Z* and *E* isomer contents are (98.5%:1.5%) and (11.5%:88.5%), for the *Z*-enriched and *E*-enriched solutions. (C) Absorption spectra of *Z*- (black) and *E*- (red) enriched solutions of ZW-NAIP used in the transient experiments. The blue curve is the difference between both spectra. The blue and green arrows show the pump wavelength (400 nm) for TA experiments on both samples, and the Ar laser line (454.6 nm) used for *E*-isomer accumulation, respectively.

- At early times, excited-state absorption (ESA) has a maximum at 430 nm and extends into the near-UV, overlapping the ground-state bleach (GSB). With increasing delay time, the ESA shifts to shorter wavelengths, and is maximum at a delay of $\Delta t = 0.20$ ps in the range 320–335 nm (figure 2(B)). This dynamic blue-shift is evidence for an excited-state vibrational wavepacket, which evolves along the isomerization reaction coordinate on a barrierless excited state potential energy toward the CI.
- The UV spectroscopic signature of the wavepacket in S_1 is lost rapidly, and a subsequent ground state photoproduct absorption (PA) is observed with a prominent, red-shifted wing. Here, the term 'photoproduct' denotes the vibrationally hot *E/Z* isomer mixture generated through the excited state decay. Due to the moderate reaction quantum yield the reactant isomer configuration dominates the photoproduct. This signal is maximal at 0.39 ps at 550–600 nm, and characterizes the arrival time of the vibrational wavepacket in

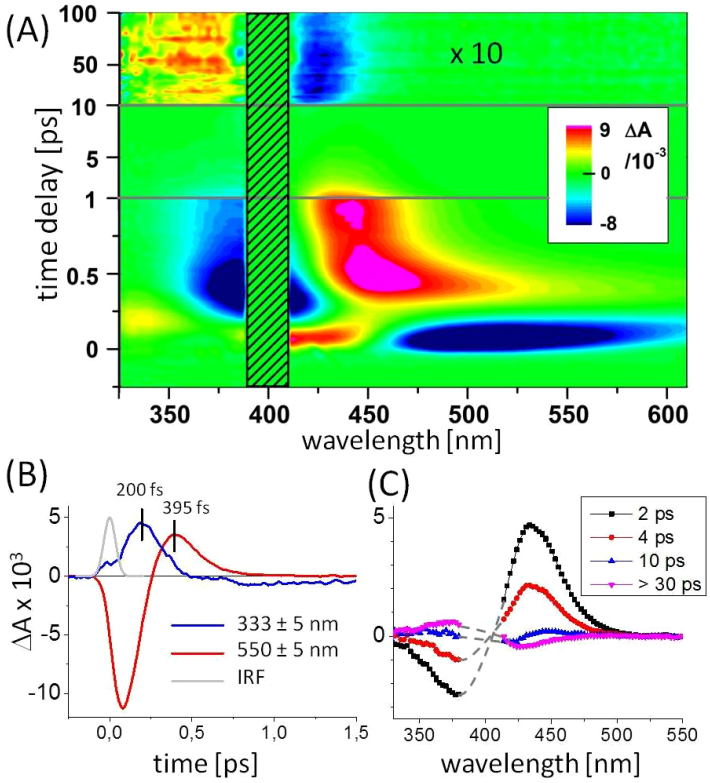

Figure 2. (A) Two-dimensional plot of the TA signal (in false colors) of *Z*-ZW-NAIP in CD_3OD as a function of probe wavelength (from 320 to 610 nm) and pump–probe delay (from −0.25 to 100 ps). The data is processed to correct for the solvent contributions and for the chirp (see [19] for details). Because of enhanced noise due to pump light scattering, the crossed-out portion around 400 nm is disregarded. Note that from 10 to 100 ps, the signal is magnified ten times. (B) Selected time traces: At 333 nm, the rise of the UV most part of the ESA is delayed and slower than the instrument response function (IRF in gray). It is maximal at 200 ± 20 fs. At 550 nm, the early SE rapidly decays to give rise to an unthermalized photoproduct signature, maximum at 390 ± 20 fs. (C) Spectral evolution from the vibrationally 'hot' ground state populations with a max. at 430 nm to the final equilibrated *E*–*Z* difference spectrum after 30 ps.

this spectroscopic observation window of the photoproduct S_0 state. The crossover between SE and PA in the red most part of the TA data is attributed to the signature of the passage of the molecular system through the CI [19], in line with similar observations in Rh [18].

- The PA band rapidly narrows (blue shifts) and ΔA evolves ($\Delta t \geqslant 0.5$ ps) into a difference spectrum with a pronounced GSB below 400 nm, and a positive lobe around 430 nm characteristic of vibrationally excited ground state species (figure 2(C)).
- Kinetic traces taken at the red and blue wings of the ground state absorption spectrum display anti-phased oscillations with a 650 ± 50 fs period ($\sim 50 \pm 5\ cm^{-1}$) and 270 fs damping time (see supplementary data, available from stacks.iop.org/NJP/15/105022/mmedia), indicative of a ground state vibrational wavepacket [19].

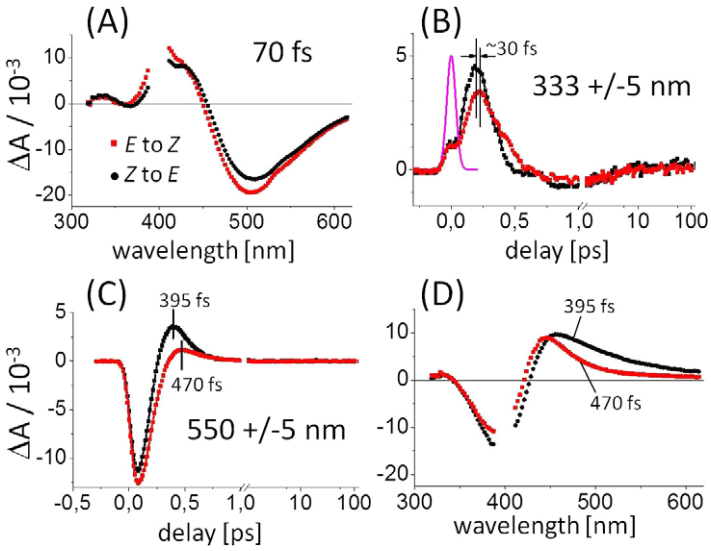

Figure 3. Comparison of the forward (black) and backward (red) isomerization reactions of ZW-NAIP in CD_3OD. (A) After 70 fs, both transient spectra are similar. (B) The dynamic spectral shift of the UV ESA is also very similar as shown by the delayed transient signals at 333 nm. The pink curve is a Gaussian function representative of the instrument response function (80 fs FWHM). The step in the rise of both traces is attributed to spurious solvent signal. (C) At 550 nm, the PA rapidly following the early SE is less intense in the backward reaction, and reaches its maximum about 70 fs later, as compared to the forward reaction. (D) At the time the red wing of the PA spectrum is maximum, it is significantly more intense and more red-shifted in the forward (spectrum at 395 fs) than in the backward reaction (spectrum at 470 nm).

- The decay of the PA is characterized by two decay times of 1.0 and 4.6 ps. Due to the small photo-chromic difference of the *Z* and *E* isomers the *E*–*Z* difference spectrum has a small amplitude and emerges only after vibrational cooling is completed (>30 ps, figure 2(C)).

3.2. Ultrafast dynamics of the backward E to Z reaction

To investigate the dynamics of the backward photoisomerization, TA experiments are performed on the *E*-enriched sample. Like for the forward reaction, the pump laser is centered at 400 nm where *E* has a 10% higher absorbance than *Z*. Hence more than 90% of the observed signal correspond to the *E* to *Z* reaction. The small amplitude contribution from the minority *Z* isomer is almost impossible to decipher as the reaction kinetics turns out to be nearly the same for both isomers. The spectral differences between both isomers are only distinguishable after complete return to the thermalized electronic ground state, that is beyond 30 ps (see below).

Two-dimensional data sets similar to those displayed in figure 2 for the forward reaction are obtained for the backward photoreaction (see SI). Figures 3 and 4 illustrate the main differences between both isomerization directions. At early times (see figure 3(A)) both photoreactions show nearly identical ESA and SE spectra, with a slight blue shift of ∼5 nm, and slightly higher

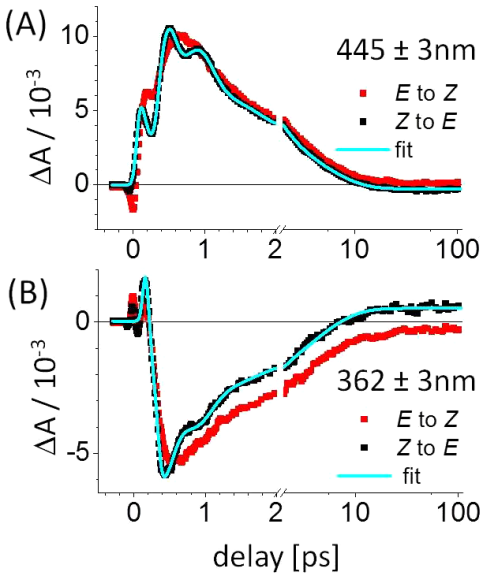

Figure 4. Comparison of kinetic traces for the forward (black) and backward (red) photoisomerization reactions of ZW-NAIP in CD_3OD at (A) 445 nm and (B) 362 nm, respectively in the low- and high-energy sides of the PA band. Note the break in time axis, with linear scale before the break and logarithmic thereafter. While the forward reaction is accompanied by an out-of-phase oscillatory behavior at both wavelengths (fit in blue, see figure S2 and table 2 below), no clear evidence of such oscillations is observed in the reverse reaction.

signal for the *E* to *Z* case, in line with the slightly stronger and blue-shifted absorbance of the *E* species. The ESA and SE kinetics are alike, indicating that the backward reaction also proceeds along a barrierless S_1 potential, topologically similar to that theoretically predicted for the forward reaction [29]. In addition, figure 3(B) shows that a dynamically blue-shifting ESA is also observed in S_1 for the backward reaction, indicative of a similar wavepacket. For the backward reaction, the maximum of the 333 nm ESA signal occurs about 30 fs later. It is also slightly weaker in amplitude and longer lived. The observed behavior suggests that the excited state PES's have similar topologies in both reaction directions and that the wave packet evolution is slightly slower and temporally defocused in the backward reaction. The ground state PA signal observed at 550 nm (figure 3(C)) is weaker and arrives later by 70 ± 20 fs for the *E* to *Z* photoreaction. Also, the earliest spectral signature of the PA is significantly less red-shifted in the backward reaction (figure 3(D)).

However, the most significant difference between the forward and backward reactions is in the ground state coherences as shown in figure 4. For the forward reaction the GSB and PA traces at 362 and 445 nm show an oscillatory behavior, which is well fitted by a damped cosine function (coherent dynamics) on top of multiexponential (incoherent) kinetics (see supplementary data, available from stacks.iop.org/NJP/15/105022/mmedia). Instead, for the backward photoreaction, only the incoherent component is observed. More precisely, if some oscillatory signal of similar period is to be considered in the backward reaction, its amplitude is

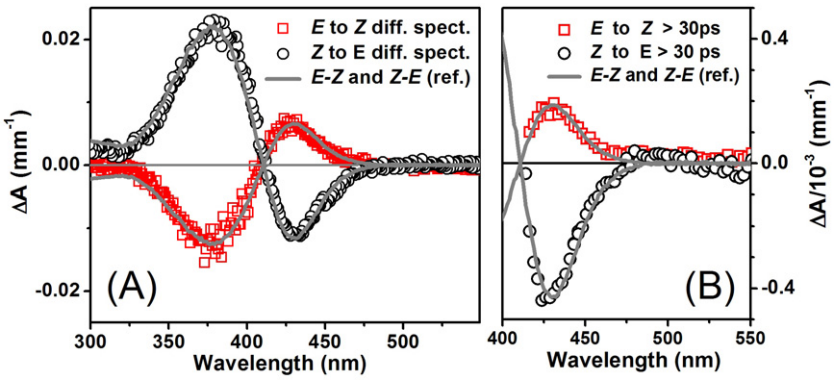

Figure 5. (A) Difference spectra of ZW-NAIP in CD_3OD comparing ground state absorbances recorded in a spectrophotometer before and immediately after 40 min TA runs. Gray lines show the static difference spectra calculated and scaled from the enriched *Z* and *E* spectra of figure 1(C). (B) Long-wavelength portion of the differential TA data recorded for ZW-NAIP in CD_3OD at long delay times (>30 ps) (open dots), compared with the static isomer difference spectra. Both spectra are mirror images of one another, provided they are scaled by the ratio of the photoisomerization yields in both directions.

within the noise level, meaning at least ∼20 times lower than in the forward direction (see the fits and residuals in figure S2 (available from stacks.iop.org/NJP/15/105022/mmedia)).

3.3. Comparison of the forward (Z → E) and backward (E → Z) isomerization yields

Figure 5 displays the final ($t > 30$ ps) difference absorption spectra observed for both forward and backward isomerization reactions. In figure 5(A), we plot the difference between the spectra of the initial *Z*-enriched and *E*-enriched samples and the spectra of the same solutions just after 40 min of experiment time in the TA set-up. The obtained *Z–E* and *E–Z* difference spectra perfectly overlap those calculated from the pure ground state absorption spectra (figure 1(C)), showing that no other photoproducts accumulate during the course of the TA experiment and that the reaction occurs reversibly in both directions. Also, their amplitudes are less than 1/10th of the reference difference spectrum (figure 1(C)), indicating that in both cases less than 10% of the molecules have undergone isomerization during the entire TA experimental time. Figure 5(B) focuses on the noiseless VIS part of stationary differential spectra obtained in the TA experiments for $t > 30$ ps. They show the characteristic signature of *Z*-enrichment or -depletion at 430 nm for the *E* to *Z* and *Z* to *E* reaction, respectively. The transient spectra also overlay perfectly with the static difference spectra, attesting that the photo-reaction is already entirely completed (and relaxed) at these time delays. Note that these data obtained with freshly synthesized photoswitches do not show the spurious photoproduct absorbing at long wavelengths that was reported in our previous work [19]. Since both initial isomer solutions have the same total concentration, the ratio of the two stationary difference spectra is the ratio of the quantum yields for the forward and backward photoreactions, multiplied by the ratio of the extinction coefficients of both isomers at the pump wavelength. We conclude that the *E* to *Z* photoisomerization yield is ∼2.5 weaker than for the *Z* to *E* photoreaction. The latter was measured to be ∼35% [19].

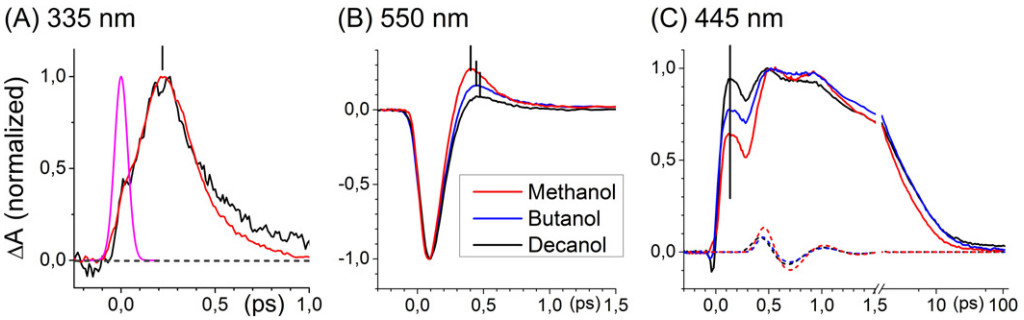

Figure 6. Selected kinetic traces comparing the *Z* to *E* photoreaction dynamics in methanol (red), butanol (blue) and decanol (black). (A) Delayed onset of the UV signature of the excited state wavepacket at 335 nm in methanol and decanol only. The purple line represents the IRF. (B) SE, followed by the delayed onset of the ground state photoproduct signature at 550 nm. Vertical lines around 0.4–0.47 ps indicate the arrival times of the wavepacket in the ground state. (C) ESA (pinpointed by the vertical line) followed by the oscillating signature of the ground state photoproduct at 445 nm. The dashed lines are the oscillatory components extracted from the fit (see supplementary data, available from stacks.iop.org/NJP/15/105022/mmedia and table 2 below). Note that 445 nm is the region of cross over between ESA signal ($\lambda < 445$ nm) and SE ($\lambda > 445$ nm) at early times. Minor, solvent-induced spectral shift of this crossover is responsible for the apparent difference in the early ESA signal amplitude.

3.4. Solvent effects on the forward reaction

We studied the TA signals for the *Z* to *E* photoreaction for a limited set of alcohols with increasing alkyl chain length and viscosity (in Pa s at 25 °C) [31] methanol (0.54 Pa s), butan-1-ol (2.54 Pa s) and decan-1-ol (10.9 Pa s). The zwitterionic chromophore displays a very weak solvatochromism, as only a 2 nm blue shift is observed in the absorption spectra when *Z*-ZW-NAIP is dissolved in decanol (not shown). The same is true for the ESA and transient ground state spectra. Hence we assume that a given probe wavelength characterizes the same transient molecular state and geometry whatever the solvent. Some of these kinetic traces are highlighted in figure 6. The signature of vibrational coherence such as the delayed onset of the ESA in the UV (figure 6(A)), the delayed onset of the PA signature which is maximum at 0.4–0.45 ps (figure 6(B)) and the ground state oscillations after 0.4 ps (figure 6(C)) are observed to be rather independent of the solvent. The amplitude of the oscillatory signal seems to be slightly reduced in butanol and decanol compared to what it is in decanol but their period and damping are the same within the experimental accuracy (see below). We conclude that the vibrational dynamics and photoreaction speed are hardly affected by the local viscosity which increases by a factor ∼20 from methanol to decanol. This lack of influence indicates that the reaction coordinate operating in these system is at least partially 'space saving'. Such reaction coordinate would be characterized by a combination of skeletal torsional deformation (e.g. the dihedral angle $C_5C_4C_{1'}C_{9'}$) and ring inversions as already described in previous reports [20, 29], to minimize the volume required for completing the double bond isomerization. In particular,

Table 1. A global analysis of the TA data after 1.2 ps (see the SI of [19] for technical details) reveals that the vibrational relaxation in the ground state is well characterized by two time constants in all experiments reported here. The first three lines show results which all agree within the estimated error bar of 10%. The last two lines show significantly longer time constants, due to the solvent influence.

	τ_1 (ps)	τ_2 (ps)
Z-ZW-NAIP in CH_3OH[a]	1.2	4.8
Z-ZW-NAIP in CD_3OD	1.0	4.6
E-ZW-NAIP in CD_3OD	1.3	5.1
Z-ZW-NAIP in $CH_3(CH_2)_3OH$	1.6	7.1
Z-ZW-NAIP in $CH_3(CH_2)_9OH$	2.0	7.5

[a] Results from [19].

the ring inversion motion would involve pyramidalization at the C_4 and $C_{1'}$ centers which help to accomplish the isomerization reaction even in a situation where the skeletal deformation is more limited. Such mixed reaction coordinate is reminiscent of the space saving bicycle-pedal reaction coordinate proposed and computationally detected in Rh [26].

3.5. Quantitative analysis of the TA kinetics

For all TA data presented in this work, a quantitative analysis has been carried out according to the procedures already described previously [19, 20]. In particular, the same global analysis was applied to analyze the spectral relaxation induced by incoherent, ground state vibrational relaxation at time delays larger than 1.2 ps. This relaxation is depicted in figure 2(C) in the case of *Z*-ZW-NAIP in deuterated methanol. In all cases a similar spectral relaxation is observed which proceeds with two time constants summarized in table 1. The results of the analysis are twofold. Firstly we observe that in deuterated methanol the vibrational relaxation proceeds with almost the same time constants for the forward (1.0 and 4.6 ps) and backward (1.3 and 5.1 ps) reactions. Secondly, it is slower in the less polar, longer-chain alcohols, with 30–40% longer characteristic times in decanol. These results confirm that the spectral relaxation observed at time delays >1.2 ps is due to vibrational energy dissipation and/or dielectric relaxation involving the solvent, with slower dipolar solvation [32] and reduced heat dissipation in longer-chain alcohols.

Regarding the coherent dynamics, the choice of the fitting function is a critical issue in such a case where dynamic spectral shifts, delayed components and oscillatory signals are observed. Here, all the observed oscillatory features have been analyzed using the same fitting function as already described in detail (see supplementary data, available from stacks.iop.org/NJP/15/105022/mmedia and [20]). Table 2 summarizes the periods and damping times of the oscillatory compounds observed on the various experimental conditions realized here. It reveals that, the solvent viscosity does not affect the oscillation period (650–720 fs in all cases) nor the damping (250–350 fs) beyond the error bars on these values.

Table 2. Period (T_{osc}) and damping time (τ_{osc}) obtained from the fitting of the oscillatory features observed in TA data (see supplementary data, available from stacks.iop.org/NJP/15/105022/mmedia). The error bar is estimated to be 10% on the periods and up to 25% on the damping times, due to the limited signal-to-noise ratio and to the rapid damping of the oscillations.

	T_{osc} (fs)	τ_{osc} (fs)
Z-ZW-NAIP in CH_3OH (see SI)	650	270
Z-ZW-NAIP in CD_3OD	700[a]	290[a]
E-ZW-NAIP in CD_3OD	–	–
Z-ZW-NAIP in $CH_3(CH_2)_3OH$	660	360
Z-ZW-NAIP in $CH_3(CH_2)_9OH$	720	250

[a] Results of the fit displayed in figure 4 (see also the SI, figure S2).

4. Discussion

The TA signatures of the excited state dynamics of the ZW-NAIP starting either from the *E*- or the *Z*-Franck–Condon states are like in other IP compounds where ground state vibrational coherence is observed [19, 20]. In all cases, the excited state deactivation is very rapid, with non-exponential kinetic traces (at 320–340 nm) featuring a dynamic blue-shift of the ESA ($S_1 - S_n$ absorption), and a shorter-lived SE (S_1–S_0 transition). This is a direct fingerprint of an excited state wavepacket, which can be probed with its $S_1 - S_n$ absorption during its progression along the reaction coordinate on a barrierless excited state potential energy surface [19, 20, 27–29]. Instead, the $S_1 - S_0$ transition dipole moment probes a smaller region of the configuration space close to the Franck–Condon region, in line with the prediction of a rapid drop of the $S_1 - S_0$ transition dipole moment along the reactive motion [20]. Note that observing ESA lifetimes longer than SE decay is not uncommon [16].

In the IP compounds, the observation of a dynamic blue shift, rather than excited-state oscillations like in other photoisomerizing molecules, indicates that the wavepacket does not bounce back, but drops irreversibly into the CI seam after the first $\approx 90^\circ$ dihedral angle change. This physical picture is further supported by the sudden crossover between SE and PA in the red edge of the detection window and subsequent blue shift of the PA, which are qualitatively the same as the prototypical behavior reported for the coherent photoisomerization of Rh, and indicate the passage of a vibrationally coherent population through the CI [18]. Finally, as already argued [19, 20] in the case of Z-ZW-NAIP, the observed oscillations are attributed to a ground state vibrational wavepacket which most likely results from the reactive motion in the excited-state, rather than from a resonant impulsive stimulated Raman scattering process [2, 4, 33]. Hence the vibrational coherence appears to be preserved after the decay to the ground state. In the case of the cationic *Z*-MeO-NHIP as well as *Z*- and *E*- MeO-NAIP, very similar ground state oscillations are observed and have been assigned to ring deformations (in particular inversions at C_3), which contribute to the reaction coordinate and are triggered by the reactive motion in the excited state [20]. The present observation on *Z*-ZW-NAIP, that the period and damping of the oscillations accompanying the forward reaction are not affected by a 20-fold increase of the solvent viscosity further supports the assignment to such a space saving mode.

Remarkably, in the case of *E*-ZW-NAIP, despite a very similar coherent excited-state dynamics, and a similar photoproduct appearance time (470 versus 400 fs for the forward reaction, see figure 3(A)) the quantum yield is 2.5 times lower and no vibrational coherence is detected in the photoproduct state. These two observations have important implications.

First of all, invoking the Landau–Zener (LZ) model for non-adiabatic transitions it has been argued that the high photoisomerization speed of Rh would be responsible for its high quantum yield [1]. In the case of azobenzene (AB) and AB derivatives [16] it is indeed observed that the reaction speed correlates with the quantum yield. However, in other retinal proteins where the all-*trans* to 13 *cis* and reverse photoisomerizations of retinal are involved, it is observed that the fastest photoreaction is the less efficient [34]. In the IP molecular switches also, it has been observed that a very high photoreaction speed (<300 fs) is not sufficient to achieve a very high isomerization yield, which is only $\sim$20% in the case of the cationic MeO-NAIP [28]. Conversely, a 'de-methylated' MeO-NAIP, where C_5 carries a hydrogen atom rather than a methyl group, was reported to have a longer excited-state lifetime and a similar quantum yield [30] as compared to the parent MeO-NAIP [28]. Also, experiments on retinal in solution evidenced that methylation of the carbon backbone simultaneously reduces the excited-state lifetime and the photoisomerization quantum yield [35], or that the quantum yield is influenced by the solvent, without any clear correlation to the reaction speed [36]. Here, we discuss a case where in both isomerization directions, the early excited state dynamics and photoreaction speeds are almost equal, pointing to very similar PES topologies, but the quantum yields differ by a factor of 2.5. Hence, as already described by the LZ model [37], not only the reaction speed governs the quantum yield, but certainly also the details of the topology of the PES (which is taken into account in the LZ model by the difference in the PES slopes) and their coupling in the vicinity of the CI. What is more, based on the present observations, we may not even exclude that the quantum yield is influenced by further dynamics on the ground state potential soon after the CI. Such a scenario goes beyond the LZ picture and has been suggested by recent theoretical developments including dynamic electron correlations in the computation of the ground state PES of a retinal model system [38].

The second important observation is the direction-dependent occurrence of vibrational coherence in the product of the internal conversion. Previous investigations of the parent cationic MeO-NAIP revealed a similarly fast photoreaction and the occurrence of vibrational coherence in both isomerization directions [20]. This would suggest that provided the departure from the FC region and the crossing of the CI are sufficiently fast, one may observe a reaction-driven vibrational coherence in the photoproduct [33]. Instead, the 'de-methylated' dMe-MeO-NAIP, was reported to have a longer excited-state lifetime ($\sim$500 fs) and no ground state oscillations [30] (see figure 7 for atom numbering). The latter observation may be rationalized by arguing that the initial reactive motion in the excited-state is significantly slower, and in particular, slower than vibrational dephasing, which precludes the build-up of vibrational coherence along low-frequency modes. In the present case of ZW-NAIP, although the excited-state dynamics is similarly fast in both directions, vibrational coherence is observed only in one direction.

More precisely, given the relative quantum yields in both photoisomerization directions, the *Z* isomer formation yield is 0.65 (1–0.35) in the forward direction (from *Z* back to *Z*) and 0.15 only in the backward direction (from *E* to *Z*). If the vibrational coherence would be associated to the formation of the *Z* isomer only, independent of the way the population reaches the Z ground state potential well, one would see a reduction of a factor $\sim$4 in the amplitude of the oscillations

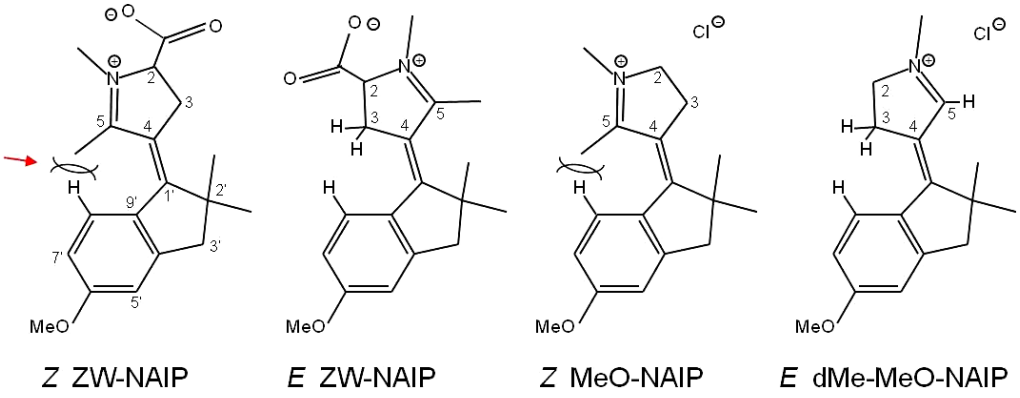

Figure 7. Schemes of the ground state structures of various NAIP compounds. In the *Z* isomer of ZW-NAIP, steric hindrance between the methyl group carried by C_5 and the hydrogen carried by $C_{8'}$ induces a 13° torsion of the $C_{1'}=C_4$ bond (see SI of [29]). In the *E*-ZW-NAIP, the methyl substitute of C_5 can fit between both methyl groups carried by $C_{2'}$, but residual stress induces significant pyramidilization of $C_{1'}$ and C_4 (among other deformations) and produces a non-planar structure too. In the case of *Z*-MeO-NAIP, the $C_{1'}=C_4$ bond is twisted by 11° in the ground state [27]. Instead in the dMe-MeO-NAIP, where C_5 carries a H atom instead of the methyl group, the *E* isomer is planar.

in the backward direction as compared to the forward direction. Given the high signal to noise ratio (S/N) achieved here (see figure S2 (available from stacks.iop.org/NJP/15/105022/mmedia) and discussion above (), the first oscillation periods, with a four-times reduced amplitude ($>0.5\times10^{-3}$), would be clearly detected on top of the noise floor ($<0.2\times10^{-3}$). Hence we conclude that although a similar vibrational wavepacket is produced by the initial fast relaxation in S_1 in both forward and backward directions (evidenced by the same dynamic blue shift of the ESA), vibrational dephasing seems to occur in the vicinity of the CI, with a damping efficiency depending on the exact pathway through the intersection seam between S_1 and S_0. In addition, the lack of influence of solvent viscosity on the period and damping of the oscillations observed in the forward direction indicates that the vibrational dephasing is essentially an intramolecular process.

As was discussed in various photoisomerizing systems [16, 39–41], different degrees of C=C twisting in the ground state may be invoked to rationalize the difference in photoreaction speeds and corollary in the occurrence of vibrational coherence. In the MeO-NAIP, the steric hindrance of the methyl group carried by C_5 induces a deviation from planarity of the molecule while in dMe-MeO-NAIP is planar in the ground state (see figure 7). Hence, in analogy with the case of the planar *E*- versus twisted *Z*- AB [39] we argue that in the case of the planar *E* isomer of dMe-MeO-NAIP, the initial reactive motion in the excited-state is significantly slower, which would possibly explain both the lower speed and lack of any wavepacket character before and after the internal conversion. In contrast, for the case of *Z*- and *E*-ZW-NAIP, both ground state structures have been computed by Melloni *et al* [29], and appear to be significantly distorted from planarity, not only due the methyl group carried by C_5, but also most likely to enhanced intramoleculer electrostatic interaction between the pyrrolinium C=N charge and the anionic carboxylate substituent. This may help rationalizing the observation that the reaction speed is

similar and an excited state wavepacket is observed for both directions, but does not reveal anything regarding the vibrational dephasing or the branching (toward the reactant and product) occurring upon decay at the CI. These may assist the building-up of low-frequency vibrational quantum coherence along the reactive molecular mode. Further experimental and theoretical studies are therefore needed to reveal the multimodal non-adiabatic evolution of the molecular ensemble.

5. Conclusion

Like other IP switches [20], the spectro-temporal signatures of the photoisomerization of ZW-NAIP shows remarkable similarities with those of retinal in Rh, including the observation of reaction driven vibration coherences in the photoproduct. It should be noted that, to the best of our knowledge, transfer of excited state coherence onto the ground state potential energy surface is not reported for any other photoisomerizing molecule in solution. Hence the IP photoswitches appear as a good model system to investigate the mechanisms that control the photoisomerization dynamics, yield and the accompanying vibrational coherence.

Here, the forward and backward reaction dynamics of the zwitterionic ZW-NAIP switch are studied by broadband TA spectroscopy with 80 fs resolution. Although the excited state dynamics and photoreaction speeds are very similar in both directions, the quantum yields are significantly different, and the vibrational coherence observed upon light excitation of the *Z* form is not observed when exciting the *E* form. We conclude that a very high isomerization speed neither enables a high quantum yield nor preserves vibrational coherence through the CI. Mechanisms usually invoked fail here to rationalize the experimental observations. In particular, we speculate that ground state dynamics, soon after crossing the CI may contribute to the determination of the quantum yield unlike the Landau–Zener physical picture. Most likely, quantum yield and vibrational dephasing are strongly influenced by the exact pathway through the intersection seam between S_1 and S_0 states. Ground state structural information does not help rationalizing these observations. This work calls for further theoretical modeling addressing specifically the mechanisms that control the photoreaction yield as well as reaction driven vibrational coherence.

Acknowledgments

Financial support is provided by the ANR grant 11-JS04-010-01 'IPQCS', the CPER Nanomat, EquipEX 'UNION'(ANR grant 10-EQPX-52) and LabEX 'NIE'. MO acknowledges support from the Université de Strasbourg for an invited professorship. SF, VZ and MO are grateful to the Italian MIUR for funding (PRIN 2010-2011).

References

[1] Wang Q *et al* 1994 Vibrationally coherent photochemistry in the femtosecond primary event of vision *Science* **266** 422–4

[2] Chesnoy J and Mokhtari A 1988 Resonant impulsive-stimulated Raman scattering on malachite green *Phys. Rev.* A **38** 3566

[3] Pollard W T *et al* 1990 Quantum-mechanical theory for 6 fs dynamic absorption spectroscopy and its application to nile blue *Chem. Phys. Lett.* **168** 239

[4] Dexheimer S L *et al* 1992 Femtosecond impulsive excitation of nonstationary vibrational states in bacteriorhodopsin *Chem. Phys. Lett.* **188** 61–6
[5] Banin U *et al* 1994 Impulsive excitation of coherent vibrational motion ground surface dynamics induced by intense short pulses *J. Chem. Phys.* **101** 8461
[6] Schoenlein R W *et al* 1991 The first step in vision: femtosecond isomerization of rhodopsin *Science* **254** 412–5
[7] Szarka A Z *et al* 1995 Vibrational coherence in the solution phase photoisomerization reaction of *cis*-stilbene *Chem. Phys. Lett.* **240** 25
[8] Takeuchi S and Tahara T 2000 Vibrational coherence of S1 *trans*-stilbene in solution observed by 40-fs-resolved absorption spectroscopy *Chem. Phys. Lett.* **326** 430–8
[9] Siewertsen R *et al* 2009 Parallel ultrafast *E–C* ring closure and *E–Z* isomerisation in a photochromic furylfulgide studied by femtosecond time-resolved spectroscopy *Phys. Chem. Chem. Phys.* **11** 5952–61
[10] Chosrowjan H *et al* 2004 Low-frequency vibrations and their role in ultrafast photoisomerization reaction dynamics of photoactive yellow protein *J. Chem. Phys.* B **108** 2686
[11] Hou B *et al* 2003 Comparing photoinduced vibrational coherences in bacteriorhodopsin and in native and locked retinal protonated Schiff bases *Chem. Phys. Lett.* **381** 549–55
[12] Kobayashi T, Saito T and Ohtani H 2001 Real-time spectroscopy of transition states in bacteriorhodopsin during retinal isomerization *Nature* **414** 531–4
[13] Kahan A *et al* 2007 Following photoinduced dynamics in bacteriorhodopsin with 7-fs impulsive vibrational spectroscopy *J. Am. Chem. Soc.* **129** 537–46
[14] Haran G *et al* 1999 Femtosecond polarized pump–probe and stimulated emission spectroscopy of the isomerization reaction of rhodopsin *J. Chem. Phys.* A **103** 2202–7
[15] Zgrablić G, Haacke S and Chergui M 2007 Vibrational coherences of the protonated Schiff base of all-*trans* retinal in solution *Chem. Phys.* **338** 168
[16] Siewertsen R *et al* 2011 Superior $Z \rightarrow E$ and $E \rightarrow Z$ photoswitching dynamics of dihydrodibenzodiazocine, a bridged azobenzene, by S1($n\pi^*$) excitation at $\lambda = 387$ and 490 nm *Phys. Chem. Chem. Phys.* **13** 1054–63
[17] Ioffe I *et al* 2011 Photoisomerization around a fulvene double bond: coherent population transfer to the electronic ground state? *ChemPhysChem.* **12** 1860–71
[18] Polli D *et al* 2010 Conical intersection dynamics of the primary photoisomerization event in vision *Nature* **467** 440-U88
[19] Briand J *et al* 2010 Coherent ultrafast torsional motion and isomerization of a biomimetic dipolar photoswitch *Phys. Chem. Chem. Phys.* **12** 3178–87
[20] Léonard J *et al* 2012 Mechanistic origin of the vibrational coherence accompanying the photoreaction of biomimetic molecular switches *Chemistry* **18** 15296–304
[21] Conyard J *et al* 2012 Ultrafast dynamics in the power stroke of a molecular rotary motor *Nature Chem.* **4** 547–51
[22] Wurzer A J *et al* 1999 Comprehensive measurement of the S1 azulene relaxation dynamics and observation of vibrational wavepacket motion *Chem. Phys. Lett.* **299** 296
[23] Banin U and Ruhman S 1993 Ultrafast photodissociation of I_3[sub 3]. Coherent photochemistry in solution *J. Chem. Phys.* **98** 4391
[24] Rosca F *et al* 2000 Investigations of coherent vibrational oscillations in myoglobin *J. Phys. Chem.* A **104** 4280–90
[25] Frutos L M *et al* 2007 Tracking the excited-state time evolution of the visual pigment with multiconfigurational quantum chemistry *Proc. Natl Acad. Sci. USA* **104** 7764–9
[26] Schapiro I *et al* 2011 The ultrafast photoisomerizations of rhodopsin and bathorhodopsin are modulated by bond length alternation and HOOP driven electronic effects *J. Am. Chem. Soc.* **133** 3354
[27] Lumento F *et al* 2007 Quantum chemical modeling and preparation of a biomimetic photochemical switch *Angew. Chem. Int. Edn Engl.* **46** 414–20
[28] Sinicropi A *et al* 2008 An artificial molecular switch that mimics the visual pigment and completes its photocycle in picoseconds *Proc. Natl Acad. Sci. USA* **105** 17642–7

[29] Melloni A *et al* 2010 Modeling, preparation, and characterization of a dipole moment switch driven by *Z/E* photoisomerization *J. Am. Chem. Soc.* **132** 9310
[30] Dunkelberger A D *et al* 2012 Photoisomerization and relaxation dynamics of a structurally modified biomimetic photoswitch *J. Phys. Chem.* A **116** 3527–33
[31] Lide D R (ed) 1990 *CRC Handbook of Chemistry and Physics* (Boca Raton FL: CRC)
[32] Horng M L *et al* 1995 Subpicosecond measurements of polar solvation dynamics: coumarin 153 revisited *J. Phys. Chem.* **99** 17311–37
[33] Kumar A T N *et al* 2001 Investigations of amplitude and phase excitation profiles in femtosecond coherence spectroscopy *J. Chem. Phys.* **114** 701
[34] Wand A *et al* 2011 Asymmetric toggling of a natural photoswitch: ultrafast spectroscopy of anabaena sensory rhodopsin *J. Am. Chem. Soc.* **133** 20922–32
[35] Sovdat T *et al* 2012 Backbone modification of retinal induces protein-like excited state dynamics in solution *J. Am. Chem. Soc.* **134** 8318–20
[36] Zgrablić G, Novello A M and Parmigiani F 2011 Population branching in the conical intersection of the retinal chromophore revealed by multipulse ultrafast optical spectroscopy *J. Am. Chem. Soc.* **134** 955–61
[37] Landau L and Lifshitz E 1977 *Quantum Mechanics: Non-Relativistic Theory* (*Course of Theoretical Physics* vol 3) (Oxford: Pergamon)
[38] Gozem S *et al* 2012 Dynamic electron correlation effects on the ground state potential energy surface of a retinal chromophore model *J. Chem. Theory Comput.* **8** 4069–80
[39] Stuart C M, Frontiera R R and Mathies R A 2007 Excited-state structure and dynamics of *cis*- and *trans*-azobenzene from resonance Raman intensity analysis *J. Phys. Chem.* A **111** 12072
[40] Weingart O, Schapiro I and Buss V 2007 Photochemistry of visual pigment chromophore models by *ab initio* molecular dynamics *J. Phys. Chem.* B **111** 3782–8
[41] Wand A *et al* 2012 Ultrafast photochemistry of light-adapted and dark-adapted bacteriorhodopsin: effects of the initial retinal configuration *J. Phys. Chem.* B **116** 10444–52